IEEE Access
Multidisciplinary | Rapid Review | Open Access Journal

Received October 9, 2019, accepted October 26, 2019, date of publication October 31, 2019, date of current version November 14, 2019.

Digital Object Identifier 10.1109/ACCESS.2019.2950692

A Novel Type of Stochastic Resonance Potential Well Model and Its Application

SHANGBIN JIAO [1,2], SHUANG LEI [1], WEI JIANG [1], QING ZHANG [1], AND WEICHAO HUANG [1,2]

[1]Shaanxi Key Laboratory of Complex System Control and Intelligent Information Processing, Xi'an University of Technology, Xi'an 710048, China
[2]National and Local Joint Engineering Research Center of Crystal Growth Equipment and System Integration, Xi'an 710048, China

Corresponding author: Shuang Lei (997232409@qq.com)

This work was supported in part by the Program of National Natural Science Foundation of China under Grant 61871318, in part by the Key Program of National Natural Science Foundation of China under Grant 61533014, and in part by the Key Research Program of Shaanxi Province under Grant 2019GY-099.

ABSTRACT For a stochastic resonance system, the characteristics of the nonlinear model have an important influence on the output. To further improve the enhanced detection of stochastic resonance, a novel potential well stochastic resonance model is constructed to simultaneously solve the problem of the output saturation and high barrier in the classical bistable model. Analytical expressions of the Kramers rate and output signal-to-noise ratio are presented, and weak signal detection is theoretically analyzed. The performance of the system based on the novel potential well model is simulated and analyzed. Finally, the proposed model is used for the detection of multiple high-frequency weak signals in an α-stable noise environment and a practical bearing fault signal. The simulation and experimental results demonstrate that the output of the stochastic resonance system proposed in this paper exhibits a large output signal-to-noise ratio and a high spectral peak at the characteristic frequency.

INDEX TERMS Stochastic resonance, novel potential well model, output saturation, high barrier, Kramers rate, signal-to-noise ratio, α-stable noise, bearing fault diagnosis.

I. INTRODUCTION

Stochastic resonance (SR) was proposed by Benzi in 1981 to study the problem of Earth's palaeometeorological glaciers, which well explained the periodic alternations of ice ages and warm climate periods [1], [2]. It is a nonlinear phenomenon that uses noise to enhance the detection of weak characteristic signals. The principle is that the Brownian particles undergo a nonlinear potential function to transfer partial noise energy to the signal [3].

Since the emergence of SR, the subject has attracted the interest of many scholars. The early theoretical research and simulation analysis of SR were achieved for the classical bistable model and have since made great progress [4]–[6]. To improve the enhancement performance of SR, time-delay [7], superthreshold [8], array [9], cascade [10], second-order matched [11] and coupled [12] bistable SR systems have appeared, and the simulation results have shown that detection performance is improved with these models. After a thorough theoretical study of the classical bistable model, scholars applied the classical bistable SR (CBSR) system to address mechanical fault characteristic signals [13]–[15], optical signals [16], medical signals [17], and circadian rhythms [18], [19], achieving good results.

With the deepening of the theory and application of the classical bistable model, the classical bistable model has suffered from the problem that the output is easily saturated [20] and the potential function barrier is higher [21]. Considering the problem of the classical bistable model, scholars have found that changing the potential well model is very helpful in improving the detection performance of SR, so a series of improved models of a bistable SR have been developed. Combining the Woods-Saxon model with the Gaussian potential model, a new SR model capable of independently adjusting the barrier height was obtained, which addresses the problem of the higher barrier [21]. The classical bistable model and the Gaussian potential model were combined to obtain a power-function tristable SR model, which reduces the barrier height and makes it easier to switch Brownian particles between steady states [22]. When using the stochastic resonance characteristics, Xin and Xue [23] added an additional signal to the potential function of the classical

The associate editor coordinating the review of this manuscript and approving it for publication was Gerard-Andre Capolino.

bistable model, making it easier for particles to cross the barrier. At present, the models that are employed to solve the output saturation problem are mostly piecewise bistable potential models [20], [24]–[26]. The approach taken by such piecewise nonlinear SR models is to reduce the steepness of the potential well walls in the classical bistable model so that the output is not clamped between steady-state points. In [26], a new unsaturated piecewise nonlinear bistable system was established, and the system performance was analyzed for the case of multiplicative and additive noise. The simulation results showed that piecewise bistable potential models can solve the output saturation problem and exhibit a good weak signal enhancement and anti-noise characteristics. However, the above models only address one shortcoming in the classical bistable model. Therefore, a novel potential well SR (NPWSR) model is proposed based on the piecewise bistable potential model and the applied signal stochastic resonance model to simultaneously solve the problems of the output saturation and high barrier in the classical bistable model.

The remainder of this paper is organized as follows: Section II details the piecewise bistable potential model and the applied signal SR model. Section III establishes a novel potential well model, analyzes the model theoretically, and presents the detection process based on the NPWSR model. Section IV considers α-stable noise as the noise background to analyze the system performance. Section V considers the detection of multiple high-frequency weak signals in the α-stable noise environment and a practical bearing fault signal by using the novel potential well model. The conclusions are presented in section VI.

II. POTENTIAL MODEL

A. PIECEWISE BISTABLE POTENTIAL MODEL

The classical bistable system under the action of noise $n(t)$ and an external periodic force $A\cos(\omega t)$ can be described by the following equation.

$$\mathrm{d}x/\mathrm{d}t = a_1 x - b_1 x^3 + A\cos(\omega t) + \sqrt{2D}n(t) \tag{1}$$

where $a_1 x - b_1 x^3$ is the derivative of the classical bistable model potential function, $A\cos(\omega t)$ is the external periodic force, $n(t)$ is Gaussian white noise, and D is the noise intensity. Assuming that the noise D is 0 and the signal amplitude A is 0, when $t>0$, by solving Eq. (1), the output x can be obtained as [20], [26]:

$$x = \sqrt{(a_1/(b_1 + e^{-2a_1 t}))} \tag{2}$$

We can see from Eq. (2) that x has a limit value. When $t = 0$, $x = \sqrt{(a_1/(1+b_1))}$ can be obtained. When t tends to positive infinity, x tends to $\sqrt{(a_1/b_1)}$. For the values of the three groups a_1 and b_1, the curve of x as a function of t ($t>0$) is shown in Fig. 1. Fig. 1 shows that x gradually approaches a fixed value as t increases, which is a phenomenon known as output saturation. Because there is a quadratic term of x in the classical bistable potential function, when the system

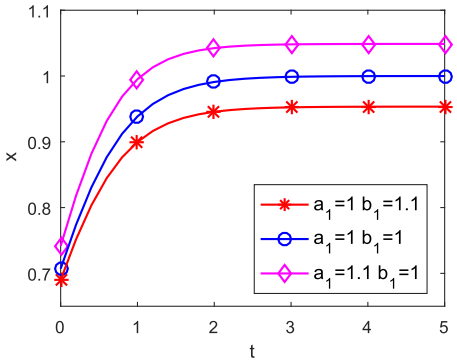

FIGURE 1. The output saturation phenomena of the CBSR system for three groups system parameters ($t>0$, for an amplitude of $A = 0$ and a frequency of $f = 0$ Hz, the purple line-x versus t for $a_1 = 1.1$ and $b_1 = 1$, the blue line-x versus t for $a_1 = 1$ and $b_1 = 1$, the red line-x versus t for $a_1 = 1$ and $b_1 = 1.1$).

responds with $x>1$, the steepness of the wall of the potential well of the classical bistable potential model is multiplied, causing the particle motion to saturate. The output saturation will limit the enhancement of weak signals by the SR and the anti-interference ability of the system.

To solve the output saturation problem of the classical bistable model, a novel piecewise bistable potential model is established, as shown in Eq. (3). This model simplifies the parameters of the piecewise bistable potential model and shortens the time required for parameter optimization.

$$U(x) = \begin{cases} -\sqrt{2}\dfrac{U_{o1}}{m_1}(x+m_1) - U_{o1} & x < -m \\ -\dfrac{1}{2}a_2x^2 + \dfrac{1}{4}b_2x^4 & -m \le x < 0 \\ -\dfrac{1}{2}a_2x^2 + \dfrac{1}{4}b_2x^4 & 0 \le x < m \\ \sqrt{2}\dfrac{U_{o1}}{m_1}(x-m_1) - U_{o1} & x > m \end{cases} \tag{3}$$

where a_2 and b_2 are system parameters, $m_1 = \sqrt{a_2/b_2}$, and $U_{o1} = a_2^2/4b_2$. To intuitively explain the improvement in the output saturation phenomenon by the piecewise bistable potential model, $a_2 = 1$, $b_2 = 1$, $D = 0$, and $s(t) = A\cos(\omega t)$ are considered in the classical bistable system and the piecewise bistable SR system, where A is 0.8, 1, 1.2, 1.6, and 2, and $\omega = 0.02\pi$. The output signals of the two systems are shown in Fig. 2. We can see from Fig. 2(a) that the amplitude of the output signal of the classical bistable system is clamped, and we can observe from Fig. 2(b) that the system is sensitive to the input signal amplitude and that the output signal amplitude is linearly amplified, effectively solving the output saturation problem of the classical bistable system.

B. APPLIED SIGNAL STOCHASTIC RESONANCE MODEL

When the system is only driven by weak periodic forces, the Brownian particles do not have enough energy to cross the barrier and oscillate between the wells, and thus the best detection results cannot be obtained. To reduce the barrier

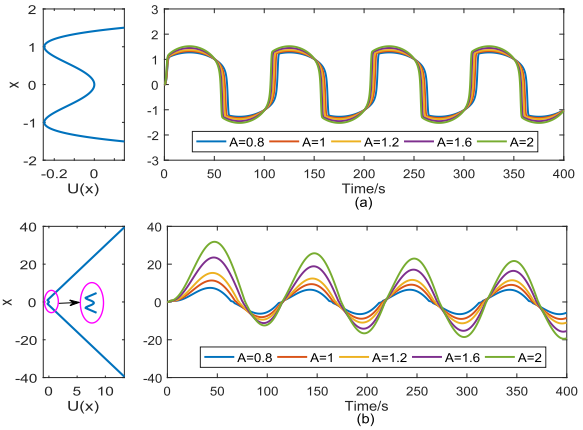

FIGURE 2. Output signals using both the CBSR system and piecewise bistable SR system for different input signal amplitudes ($D = 0$, for the amplitudes of $A = 0.8$, $A = 1$, $A = 1.2$, $A = 1.6$ and $A = 2$, and $\omega = 0.02\pi$), (a) the output signal of the CBSR system (for the system parameters $a_1 = 1$ and $b_1 = 1$); (b) the output signal of the piecewise bistable SR system (for the system parameters $a_2 = 1$ and $b_2 = 1$).

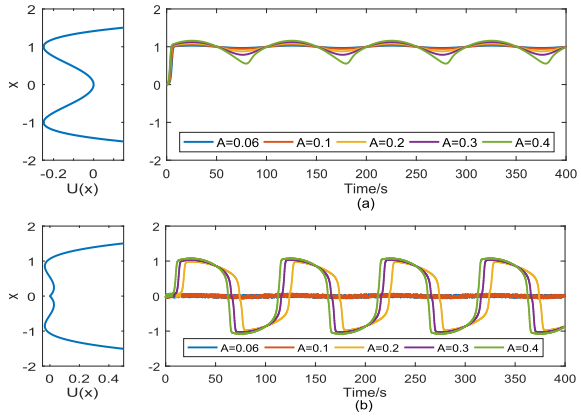

FIGURE 3. Output signals using both the CBSR system and the applied signal SR system for different input signal amplitudes ($D = 0$, for the amplitudes of $A = 0.06$, $A = 0.1$, $A = 0.2$, $A = 0.3$ and $A = 0.4$, and $\omega = 0.02\pi$), (a) the output signal of the CBSR system (for the system parameters $a_1 = 1$ and $b_1 = 1$); (b) the output signal of the applied signal SR system (for the system parameters $a_3 = 1$, $b_3 = 1$ and $l_1 = 0.6$).

height of the classical bistable model, the applied signal SR model in [23] is used so that the weak periodic signal can realize an interwell transition, and the potential function expression is shown as follows.

$$U(x) = \begin{cases} -\frac{1}{2}a_3x^2 + \frac{1}{4}b_3x^4 - A_{p1}x & x \le 0 \\ -\frac{1}{2}a_3x^2 + \frac{1}{4}b_3x^4 + A_{p1}x & x > 0 \end{cases} \tag{4}$$

where a_3 and b_3 are system parameters, $A_{p1} = l_1 \times A_{c1}$, $0 \le l_1 \le 1$, and A_{c1} is the input threshold of the system. To visualize the impact of the barrier height on the output effect, $a_3 = 1$, $b_3 = 1$, $l_1 = 0.6$, $D = 0$, and $s(t) = A\cos(\omega t)$ are considered in the classical bistable system and the applied signal SR system, where A is $0.06, 0.1, 0.2, 0.3$, and 0.4, and $\omega = 0.02\pi$. The outputs of the two systems are shown in Fig. 3. Fig. 3(a) shows that the signal with a smaller amplitude cannot cross the barrier to achieve an interwell oscillation, and optimal detection is not obtained. Fig. 3(b) shows that the applied signal SR system can lower the barrier height so that the signal with a lower amplitude can generate an interwell transition and produce a better output. However, due to the lack of noise, particles with an extremely low amplitude cannot oscillate between the wells.

III. STOCHASTIC RESONANCE SYSTEM

A. THE NOVEL POTENTIAL WELL MODEL

Under the combined action of an external force and α-stable noise, the overdamped motion of Brownian particles in SR systems can be described by Langevin's equation as:

$$\frac{dx}{dt} = -U'(x) + s(t) + \varepsilon(t) \tag{5}$$

where $x(t)$ is the system output, $U(x)$ is the potential function of the novel potential well model, $s(t)$ is a periodic(nonperiodic) signal, and $\varepsilon(t)$ is additive α-stable noise.

In this paper, $s(t)$ is shown as follows.

$$s(t) = \sum_{i=1}^{n} A_i \cos(2\pi f_i t) \tag{6}$$

where A_i is the amplitude of the *ith* signal, f_i is the frequency of the *ith* signal, and n is the number of input signals.

The novel potential well model consists of a piecewise bistable potential model and an applied signal SR model, which can solve the problems of the output saturation and high barrier in the classical bistable system. This model is linearized at $x = \pm\sqrt{a/b}$. Compared with other piecewise potential models, the novel potential well model simplifies the parameters and reduces the complexity of the parameter optimization. The potential function can be described as follows.

$$U(x) = \begin{cases} -\sqrt{2}\frac{U_o}{m}(x+m) - U_o - A_p x & x < -m \\ -\frac{1}{2}ax^2 + \frac{1}{4}bx^4 - A_p x & -m \le x < 0 \\ -\frac{1}{2}ax^2 + \frac{1}{4}bx^4 + A_p x & 0 \le x < m \\ \sqrt{2}\frac{U_o}{m}(x-m) - U_o + A_p x & x > m \end{cases} \tag{7}$$

where $m = \sqrt{a/b}$, $U_o = a^2/4b$, $A_p = l \times A_c$, $0 \le l \le 1$, A_c is the input threshold of the system, and a, b, and l are system parameters. The potential function diagram of the novel potential well model is shown in Fig. 4. We can visually see that the barrier height of the novel potential well model is lower than that of the classical bistable model, and the wall of the potential well is linearized.

The influence of the system parameters on the potential function $U(x)$ is shown in Fig. 5. Fig. 5(a) shows that the depth and width of the potential wells decrease as the parameter a decreases, and Fig. 5(b) shows that the depth and width of the potential wells increase as the

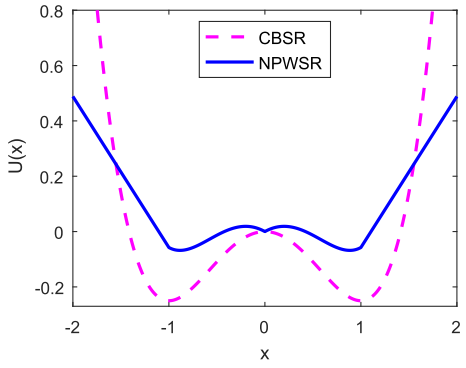

FIGURE 4. The potential functions of the NPWSR and CBSR models (the solid line-the NPWSR potential function versus x for $a = 1$, $b = 1$ and $l = 0.5$, the dotted line-the CBSR potential function versus x for $a_1 = 1$ and $b_1 = 1$).

parameter b decreases. As b increases, the multistable characteristic will be lost and gradually degenerate into a monostable characteristic. Fig. 5(c) demonstrates that the slope of the barrier wall increases as the parameter l increases and the height of the barrier decreases. An increase in the slope will result in a saturation of the output and a decrease in the height of the barrier will facilitate the transition of the particles. Therefore, when optimizing the parameters, the best matching parameters should be found to achieve the best resonance.

Substituting Eq. (7) into Eq. (5), dx/dt can be obtained as follows.

$$\frac{dx}{dt} = \begin{cases} \sqrt{2}\dfrac{U_o}{m} + A_p + s(t) + \varepsilon(t) & x < -m \\ ax - bx^3 + A_p x + s(t) + \varepsilon(t) & -m \le x < 0 \\ ax - bx^3 - A_p x + s(t) + \varepsilon(t) & 0 \le x < m \\ -\sqrt{2}\dfrac{U_o}{m} - A_p + s(t) + \varepsilon(t) & x > m \end{cases} \tag{8}$$

The novel potential well model is analyzed from the Kramers rate (r_k) and output signal-to-noise ratio (SNR) in this paper. r_k [27] is defined as the rate at which a transition occurs between the steady states of the potential function, which reflects the ability of the output signal to follow a noisy input signal. When the nonlinear system is only affected by noise, the Brownian particles switch between the steady states according to r_k in the potential wells. r_k is numerically the reciprocal of the mean first passage time, and r_k of the classical bistable model can be described as follows.

$$r_k = \frac{a_1}{\sqrt{\pi}} \exp \frac{-a_1^2}{4Db_1} \tag{9}$$

The escape problem based on the Kramers rate is that the system starts from a steady-state point and escapes the potential function potential well under the action of some forces. We solved the steady-state point of Eq. (5). The steady-state solution is $x = \pm\sqrt{a/b}$ when $l = 0$.

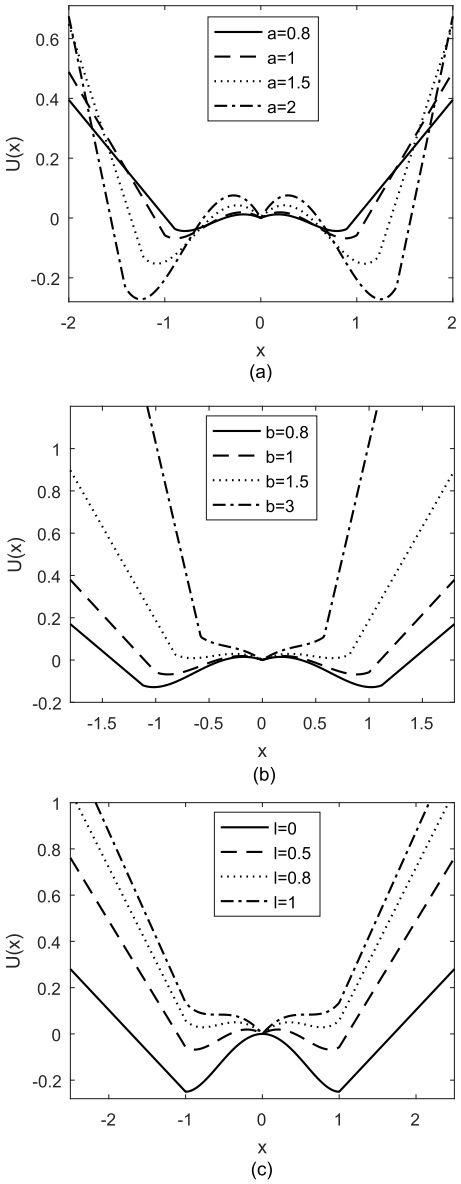

FIGURE 5. Influence of the system parameters on the potential function $U(x)$, (a) the influence of parameter a on $U(x)$ ($b = 1$ and $l = 0.5$); (b) the influence of parameter b on $U(x)$ ($a = 1$ and $l = 0.5$); (c) the influence of parameter l on $U(x)$ ($a = 1$ and $b = 1$).

When $0 \le l \le 1$, the analytical solution of the steady-state point is a complex solution that is more complicated. Therefore, we only discuss r_k in the case of $l = 0$. When $l = 0$, the novel potential well model is as follows.

$$U(x) = \begin{cases} -\sqrt{2}\dfrac{U_o}{m}(x+m) - U_o & x < -m \\ -\dfrac{1}{2}ax^2 + \dfrac{1}{4}bx^4 & -m \le x < 0 \\ -\dfrac{1}{2}ax^2 + \dfrac{1}{4}bx^4 & 0 \le x < m \\ \sqrt{2}\dfrac{U_o}{m}(x-m) - U_o & x > m \end{cases} \tag{10}$$

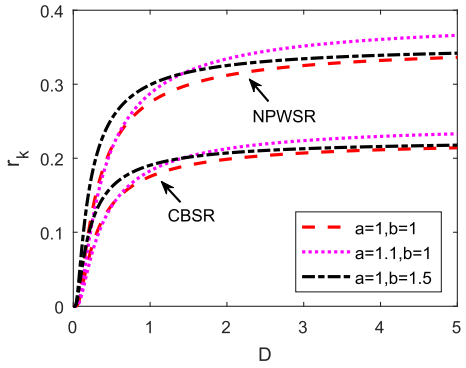

FIGURE 6. The Kramers rate r_k of the NPWSR and the CBSR models versus D for different system parameters ($l = 0$, the red line-the r_k for $a = a_1 = 1$ and $b = b_1 = 1$, the purple line-the r_k for $a = a_1 = 1.1$ and $b = b_1 = 1$, the black line-the r_k for $a = a_1 = 1$ and $b = b_1 = 1.5$).

The mean first passage time can be calculated as follows.

$$\tau_- = \frac{1}{D}\left[\int_{-m}^{-\sqrt{a/b}} \exp\left[-\sqrt{2}\frac{U_o}{m}(x+m) - U_o\right]dx\right] \cdot \left[\int_{-\sqrt{a/b}}^{0} \exp\left[\frac{1}{D}(-\frac{1}{2}ax^2 + \frac{1}{4}bx^4)dx\right]\right] \quad (11)$$

Assuming that the input signal satisfies the adiabatic approximation theory condition, using a Taylor series to expand Eq. (11), only the constant continuous term is obtained, and the mean first passage time is obtained as:

$$\tau_- \approx \frac{m\sqrt{a/b}}{\sqrt{2}U_0} exp(a^2/4bD) \quad (12)$$

$\tau_+ = \tau_-$, and r_k of the novel potential well model when $l = 0$ can be calculated as:

$$r_k = 1/\tau_\pm = \frac{\sqrt{2}U_0}{m\sqrt{a/b}} exp(-a^2/4bD) = \frac{\sqrt{2}a}{4} exp(-a^2/4bD) \quad (13)$$

To more intuitively compare the values of r_k in the novel potential well model and the classical bistable model, the distribution relationships between r_k and noise intensity are plotted for three sets of system parameters, as shown in Fig. 6. We can see from Fig. 6 that when $l = 0$, r_k of the novel potential well model is larger than that of the classical bistable model for different parameters, indicating that the model has a stronger ability to follow the resonance output of the system.

The output SNR is an important basis for judging the occurrence of SR and can reflect the effect of the system to detect a weak characteristic signal. The output SNR of the classical bistable model [3] is obtained as follows.

$$SNR = \frac{\pi}{2}\left(\frac{Ax_m}{D}\right)^2 r_k = \frac{\sqrt{2}a_1^2A^2}{4bD^2} exp\left(-\frac{a^2}{4bD}\right) \quad (14)$$

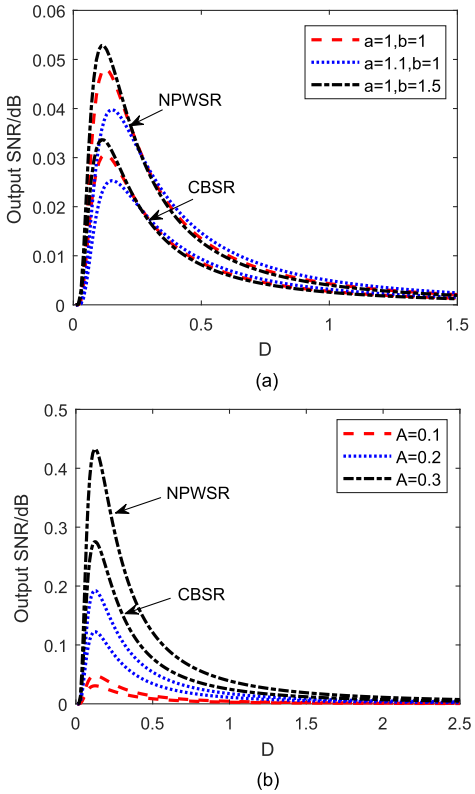

FIGURE 7. The output SNR of the NPWSR and CBSR models versus D ($l = 0$), (a) the output SNR for different system parameters (the red line-the output SNR for $a = a_1 = 1$ and $b = b_1 = 1$, the blue line-the output SNR for $a = a_1 = 1.1$ and $b = b_1 = 1$, the black line-the output SNR for $a = a_1 = 1$ and $b = b_1 = 1.5$); (b) the output SNR for different signal amplitudes (the red line-the output SNR for $A = 0.1$, the blue line-the output SNR for $A = 0.2$, the black line-the output SNR for $A = 0.3$, for the two system parameters $a = a_1 = 1$ and $b = b_1 = 1$).

where $x_m = \sqrt{a/b}$, A is the amplitude of the signal, and D is the noise intensity. The output SNR of the novel potential well model is calculated as:

$$SNR = \frac{\pi}{2}\left(\frac{Ax_m}{D}\right)^2 r_k = \frac{\pi}{2}\left(\frac{A\sqrt{a/b}}{D}\right)^2 \times \frac{\sqrt{2}U_0}{m\sqrt{a/b}} exp(-a^2/4bD) = \frac{\sqrt{2}A^2a^2\pi}{8bD} exp(-a^2/4bD) \quad (15)$$

To compare the output SNR of the novel potential well model and the classical bistable model, the distribution relationships between the output SNR and noise intensity D for different parameters and different signal amplitudes are plotted separately, as shown in Fig. 7. When $l = 0$, we can see from Fig. 7(a) that the output SNR of the novel potential well model is larger than that of the classical bistable model for different parameters, and we observe from Fig. 7(b) that the output SNR of the novel potential well model is larger than that of the classical bistable model for different signal amplitudes, which theoretically shows that the novel potential well model achieves better detection.

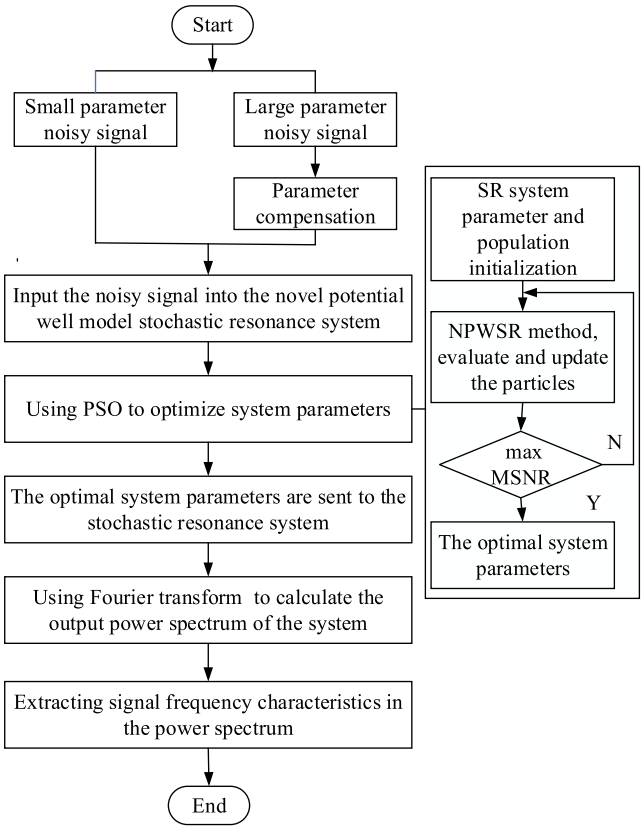

FIGURE 8. The weak characteristic signal detection process of SR system based on the NPWSR model (the part of the PSO optimization parameters is illustrated in detail).

B. OUTPUT MEASUREMENT INDEX AND DETECTION SCHEME

To reflect the effect of the SR system to detect a weak characteristic signal based on the novel potential well model, the output SNR is used as a measure. The numerical calculation of the SNR [28] is defined as follows.

$$SNR = 10log_{10}\frac{P_0}{\sum_{i=1}^{N} P_i - P_0} \tag{16}$$

where P_0 is the power at the characteristic frequency, P_i is the power of the noise, and N is the number of sampling points. If the input of the SR system is a multi-frequency signal with noise, the mean signal-to-noise ratio (MSNR) is used to measure the overall detection performance of the SR system, and its definition is as follows.

$$MSNR = \frac{\sum_{i=1}^{n} SNR_i}{n} \tag{17}$$

where SNR_i is the SNR of the ith signal to be tested and n is the number of signals. In this paper, the novel potential well model is used to detect a simulated noisy signal and a practical bearing fault signal. The specific detection process is shown in Fig. 8.

In the detection of simulated signal detection, if the signal to be tested is the a high-frequency signal, parameter compensation [29] is used to transform the large-parameter signal into a small-parameter range signal under adiabatic approximation theory. The transformation formula is as shown in Eq. (18), and K is the compensation parameter.

$$\frac{dx}{dt} = K[-U(x)' + s(t) + \varepsilon(t)] \tag{18}$$

In this paper, α-stable noise is used as the noise environment for the simulated signal detection. The generation of α-stable noise is realized by the JW algorithm [30], as shown in Eq. (19). β is a symmetrical parameter, and its range is $[-1, 1]$. σ is a scale parameter, α is a characteristic index, and its range is $(0, 2)$. When the noise parameter α is small, the pulse characteristics of the noise are evident, causing the Brownian particles to deviate from the motion trajectory and become infinite when moving in the system. Therefore, it is necessary to artificially cut off the output according to the actual detection conditions [31].

$$X = \begin{cases} N_{\alpha,\beta,\sigma}\dfrac{\sin(\alpha(V + M_{\alpha,\beta}))}{(\cos(V))^{1/\alpha}} \\ \cdot\Big[\dfrac{\cos(V - \alpha(V + M_{\alpha,\beta}))}{W}\Big]^{\alpha(1+\alpha)} & \alpha \neq 1 \\ \dfrac{2\sigma}{\pi}\Big[(\dfrac{\pi}{2} + V\beta)\tan(V) \\ -\beta\ln\big(\dfrac{(\pi/2)W\cos(V)}{\pi/2 + V\beta}\big)\Big] + \mu & \alpha = 1 \end{cases} \tag{19}$$

When applying the SR system to detect the signal, the fourth-order Runge-Kutta algorithm [32] is used to solve Eq. (8) numerically, and the output discrete time series of the system is obtained. In this paper, the overall performance is shown by Eq. (20), and the specific application will be adjusted according to the segmentation function in the novel potential well model.

$$\begin{cases} x(n+1) = x(n) + \frac{1}{6}(k_1 + k_2 + k_3 + k_4) \\ k_1 = h(-U(x(n))' + u(n)) \\ k_2 = h(-U(x(n) + k_1/2)' + u(n)) \\ k_3 = h(-U(x(n) + k_2/2)' + u(n)) \\ k_4 = h(-U(x(n) + k_3)' + u(n)) \end{cases} \tag{20}$$

where $x(n)$ is the nth discrete sequence value of the system output, $u(n)$ is the nth sampling value of the noisy signal $u(t)$, $u(t)$ is the sum of signal $s(t)$ and noise $\varepsilon(t)$, and h is the sampling step size. The potential function can be optimally matched by adjusting the system parameters. In this paper, the particle swarm optimization (PSO) algorithm [33] optimizes the three parameters a, b, and l with the output MSNR as the fitness function to obtain the best detection results. The specific steps are as follows:

(1) SR system parameter initialization. The system parameters range are set to $a\in(0,5]$, $b\in(0,5]$, and $l\in[0,1]$.

(2) The population initialization. The number of particles is set to 30, and the maximum number of iterations I_{max} is 50. A group of particles is randomly initialized, and the current position is set as the optimal state of the particles.

(3) Individual fitness evaluation. The output MSNR is used as the fitness function to evaluate the particle fitness,

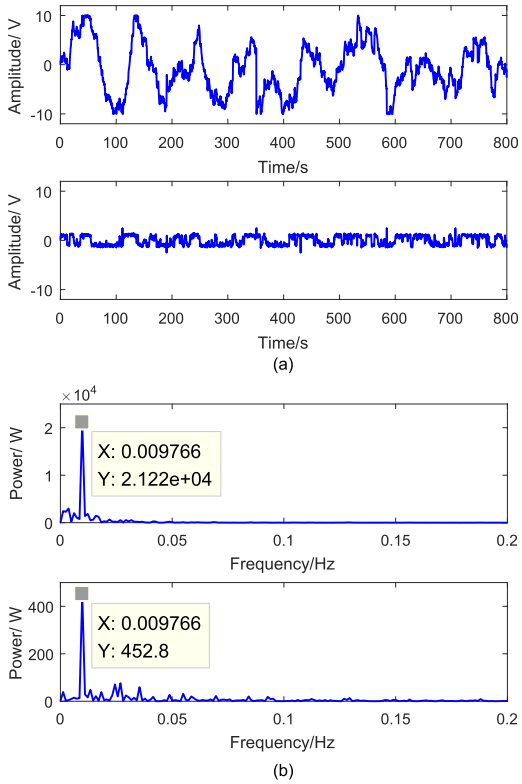

FIGURE 9. Output comparison using both the CBSR and NPWSR systems (for an amplitude of $A = 0.3$ and a frequency of $f = 0.01$ Hz), (a) the output time-domain waveform comparison; (b) the power spectrum comparison.

and the optimal position of the particle is updated by the formula in [34].

(4) Termination conditional judgment. If the current evolution algebra reaches the maximum number of iterations, then output a, b, l and the corresponding MSNR. Otherwise, the algorithm goes to step (3) to reoptimize the system parameters.

IV. SYSTEM PERFORMANCE ANALYSIS

A. SYSTEM OUTPUT

Time-domain and power spectrum diagrams of the output of the SR system can be used to visually observe the detection results. To compare the system outputs of the novel potential well model and the classical bistable model, a cosine signal with an amplitude of 0.3 and a frequency of 0.01 Hz is selected. The α-stable noise parameters are $\alpha = 1.8$, $\beta = 0$, $\sigma = 1$, and $\mu = 0$, the noise intensity is $D = 0.8$, the sampling frequency is $f_s = 5$ Hz, the data length is 4096, and the input SNR is -31.1151 dB. The noisy signal is sent into the CBSR and NPWSR systems, and the output SNR of the two systems are -8.8734 dB and -5.6262 dB. We can observe that the output SNR of the novel potential well model is higher, indicating that the obtained signal is purer. A comparison of the detection results is shown in Fig. 9. Fig. 9(a) shows that the output time-domain waveform of the novel potential well model is closer to the cosine input signal, indicating that more Brownian particles cross the barrier to achieve the interwell transition. However, the output time-domain waveform of the classical bistable model is clamped, resulting in output saturation and serious waveform distortion. We can observe from Fig. 9(b) that the output power spectrum interference components of the novel potential well model are less, and its spectral peak value is 46.9 times that of the classical bistable model, indicating that the enhanced detection performance of the novel potential well model is better.

TABLE 1. The peak ratios of the NPWSR and CBSR systems for different signal amplitudes.

A	p_2	CBSR.p_1	NPWSR.p_1	CBSR.z	NPWSR.z
0.06	15.59	608.7	1311	39.04	84.09
0.01	12.5	205	1062	16.4	84.96
0.001	12.05	372.1	939.1	30.87	77.93
0.0001	12.01	250	1108	20.81	92.25
0.00001	12.01	818.1	955.6	68.11	79.56

When the noisy signal is processed by the SR system, the power spectrum of the output signal will show a sharp peak at the frequency to be measured. According to the sensitivity of the SR to the frequency, the ratio of the spectral peak p_1 at the detection frequency in the output frequency domain to the spectral peak p_2 at the frequency corresponding to the noisy signal is defined as the peak ratio z, which is expressed as follows.

$$z = \frac{p_1}{p_2} \tag{21}$$

The magnitude of the signal influences on whether the Brownian particles can cross the barrier height. The larger the signal amplitude, the easier it is for the Brownian particles to achieve an interwell transition for the same level of noise. Therefore, it is necessary to study the output peak ratio of the system with different amplitudes for the same level of noise. We select a cosine signal with amplitudes of $A = 0.06, 0.01, 0.001, 0.0001$ and 0.00001 and a frequency of 0.01 Hz. The α-stable noise parameters are $\alpha = 2$, $\beta = 0$, $\sigma = 1$, and $\mu = 0$, the noise intensity is $D = 1.25$, the sampling frequency is $f_s = 4.89$ Hz, and the data length is 4096. The noisy signal is sent to the CBSR and NPWSR systems, and the peak ratio is obtained for different amplitudes of cosinusoidal signals, as shown in TABLE 1. We can see from the table that the NPWSR system has a higher peak ratio as the amplitude decreases, which proves that the novel potential well model is suitable for the case where the useful signal amplitude is lower.

B. WORK OF THE BROWNIAN PARTICLE

The SR system interacts with the driving force to generate work, and interacts with the noise environment to generate heat. The change in its state is accompanied by an energy transfer of both work and heat. The Brownian particles in the potential field are engaged in disordered and ordered movements, in which the work makes the particles move

in an orderly manner and the noise environment causes the particles to exhibit disordered motion. If the system can maximize the driving force, the Brownian particles will exhibit organized directional motion driven by the signal, and the effect of the thermal environment causes the system to leave the equilibrium state, which produces the SR. To compare the work of the classical bistable system and the work of the SR system based on the novel potential well model, the description of the work of the Brownian particles in [35], [36] is shown as follows.

$$W_f = \frac{1}{n}\int_{t_0}^{t_0+nT} \langle \frac{\partial U(x(t),t)}{\partial t} \rangle dt = \frac{1}{n} A\omega \int_{t_0}^{t_0+nT} \langle x(t) \cdot \sin(\omega t) \rangle dt \quad (22)$$

where W_f represents the work done by the periodic force, $T = 2\pi/\omega$ is the period of the input force, $t_0 = 0$ is the initial motion time, and $\langle \cdot \rangle$ is the overall average.

A cosine signal with an amplitude of 0.15 and a frequency of 0.01 Hz is employed. The α-stable noise parameters are $\alpha = 2$, $\beta = 0$, $\sigma = 1$, and $\mu = 0$, the sampling frequency is $f_s = 5.25$ Hz, $n = 8$, the data length is 4096 and the input SNR is -27.3208 dB. The noisy signal is sent to the CBSR and NPWSR systems, and the work of the particles as a function of the noise intensity is obtained. Because the motion of the Brownian particles in the system has strong randomness, the curve will exhibit many fluctuations that will affect the accuracy of the results. Therefore, the statistical mean value of 100 simulation experiments is used as the work of the periodic driving force, and the simulation result is shown in Fig. 10. We can see from the figure that as the noise intensity D increases, the curve of the work by the periodic force increases first and then decreases, reaching a maximum value at $D = 2.8$. Compared with the work of the classical bistable model, the work has increased by 23.8%, which indicates that the Brownian particles are more sensitive to the driving force in the NPWSR system. This result reflects the fact that the novel potential well model has a better signal detection performance than the classical bistable model.

C. OUTPUT SNR GAIN

This part of the comparison uses the signal-to-noise ratio gain (SNRG) [37], which is a measure of the signal improvement and enhancement of the system; its mathematical expression is as follows.

$$SNRG = \frac{SNR_{out}}{SNR_{in}} \quad (23)$$

where SNR_{out} is the SNR of the output signal and SNR_{in} is the SNR of the input signal. If the SNRG of the system is greater than 1, the output SNR is higher than the input SNR, and the system improves and enhances the input signal well. In this case, it can be considered that SR has occurred in the system.

To compare SNRG of the CBSR and NPWSR systems, we select a cosine signal with an amplitude of 0.4 and a frequency of 0.01 Hz as the signal to be simulated.

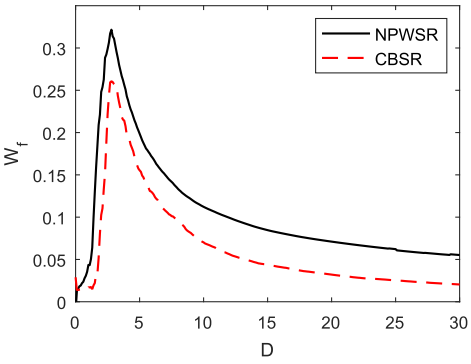

FIGURE 10. The Brown particles work W_f of the CBSR and the NPWSR systems versus D (for an amplitude of $A = 0.15$ and a frequency of $f = 0.01$ Hz, the black line-the W_f of NPWSR for $a = 1.6031$, $b = 0.6743$ and $l = 0.1238$, the red line-the W_f of CBSR for $a_1 = 3.2116$ and $b_1 = 1.707$).

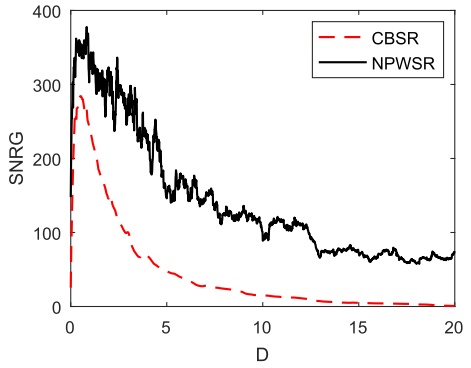

FIGURE 11. SNRG of the CBSR and NPWSR systems versus D (for an amplitude of $A = 0.4$ and a frequency of $f = 0.01$ Hz, the black line-the SNRG of NPWSR for $a = 0.2086$, $b = 0.9029$ and $l = 0.7023$, the red line-the SNRG of CBSR for $a_1 = 0.4508$ and $b_1 = 0.3691$).

The α-stable stable noise parameters are $\alpha = 1.2$, $\beta = 0$, $\sigma = 1$, and $\mu = 0$, the sampling frequency is $f_s = 4.55$ Hz, the data length is 4096 and the input SNR is -39.6759 dB. The noisy signal is sent to the two systems, and the average SNRG value of 30 simulation experiments is used to plot the curve of the noise intensity and SNRG. Fig. 11 shows that as the noise intensity D increases, the curve of the SNRG increases first and then decreases, reaching a maximum value at $D = 0.6$. The SNRG of the novel potential well model is higher for the same set of signals, indicating that the novel potential well model can obtain more information about the useful signal and that the utilization of noise is more efficient.

V. SIMULATION AND ENGINEERING APPLICATION

A. SIMULATED SIGNAL DETECTION

To verify the detection performance of the NPWSR system, the detection process shown in Fig. 8 is adopted to detect multiple high-frequency signals with an amplitude of 0.8 and frequencies of 200 Hz, 300 Hz, 400 Hz. The α-stable noise parameters are $\alpha = 1$, $\beta = 0$, $\sigma = 1$, and $\mu = 0$, the data length is 4096, the noise intensity is $D = 0.25$, the sampling frequency is $f_s = 4.55$ kHz, and the compensation parameter

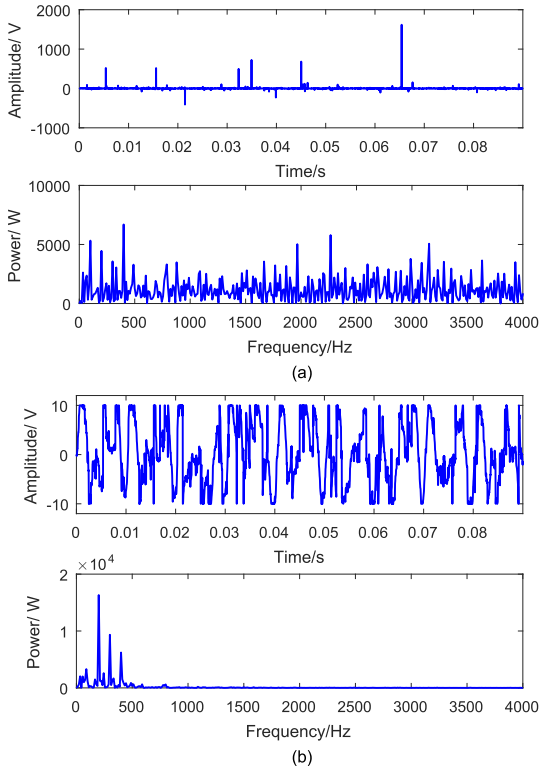

FIGURE 12. The simulated cosine signal and the corresponding power spectrum, (a) mixed signal with α-stable noise; (b) the output signal of the NPWSR system.

K is 10000. Then, we send the noisy signal (input SNR of -42.638 dB) into the NPWSR system, and the system parameters are $a = 1.1472$, $b = 0.8483$ and $l = 0.8686$ according to the PSO optimization. The detection results are shown in Fig. (12) with an output SNR of -6.638 dB. We can see that the SNR is increased by 36 dB. Fig. 12(a) demonstrates that the input signal is completely submerged by the noise and that the corresponding characteristic frequency is not observed. Fig. 12(b) shows that the output time-domain waveform is not saturated and the frequencies of 200 Hz, 299.9 Hz, 399.9 Hz can be clearly observed in the output power spectrum. The detection errors are 0%, 0.3%, 0.225%, respectively, and the error is within the acceptable range.

Fig. 13 shows the potential function curve corresponding to the system output of the simulated cosine signal. We can observe that the output signal is no longer clamped and that the particles have enough energy to carry out transitions between the wells.

B. ENGINEERING SIGNAL DETECTION

To verify the applicability of the novel potential well model to practical fault signal detection, a deep groove ball bearing (model 6205-2RS JEM SKF) is considered in this paper. The main parameters of the bearing are shown in TABLE 2 [28]. The inner and outer race signals of the faulted bearing are detected separately and compared with the detection results of the classical bistable model. The practical bearing fault data are taken from the Electrical Engineering Laboratory of

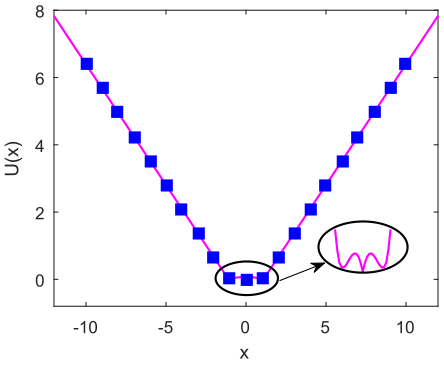

FIGURE 13. The NPWSR potential curve corresponding to the system output of the simulated cosine signal (the blue square mark is the trajectory of Brownian particle motion).

TABLE 2. Parameters of the 6205-2RS JEM SKF bearing.

d_1/inch	d_2/inch	h/inch	d/inch	D/inch	n	α/(°)
0.9843	2.0472	0.5906	0.3126	1.537	9	0

Case Western Reserve University in the United States, and the bearing drive end fault signal is selected as the signal to be tested. When the bearing is faulty, the fault characteristic frequency of the inner and outer races can theoretically be calculated according to the following formula [25], [33]:

$$f_I = 1/2 \times r/60 \times n(1 + d \times D/\cos\alpha) \quad (24)$$

$$f_o = 1/2 \times r/60 \times n(1 - d \times D/\cos\alpha) \quad (25)$$

When the fault diameter is 0.007 inch, the fault depth is 0.011 inch, and the bearing speed $r = 1772$ r/min, the fault frequency of the inner and outer races can be calculated to be 159.91 Hz and 105.86 Hz. Using the detection process shown in Fig. 8, the fault signals of the inner and outer races of the bearing are detected. Fig. 14(a) describes the waveform of the bearing inner race fault signal and its power spectrum. In the time domain diagram, the periodic characteristics cannot be clearly observed due to noise interference. In the power spectrum, the fault characteristic frequency is not observed and the frequency bands are mainly concentrated in 2500 Hz-4000 Hz. The sampling frequency is $f_s = 12$ kHz, the number of sampling points is $N = 8000$, and the input SNR is -39.13 dB. The bearing inner race fault signal is sent to the CBSR and NPWSR systems, and the parameters for the two systems are $a = 2.5205$, $b = 0.118$, $l = 0.2507$ and $a_1 = 0.2033$, $b_1 = 2.5225$ according to the PSO optimization. The detection results are shown in Figs. 14(b) and 14(c), respectively. The output SNR of the novel potential well model and the classic bistable model are -18.98 dB and -22.43 dB. We can see that the output SNR of the novel potential well model is higher. Comparing the output time-domain diagrams of Figs. 14(b) and 14(c), the periodic characteristics of the novel potential well model are more obvious. From the output power spectrum of Figs. 14(b) and 14(c), the spectral peak at the fault

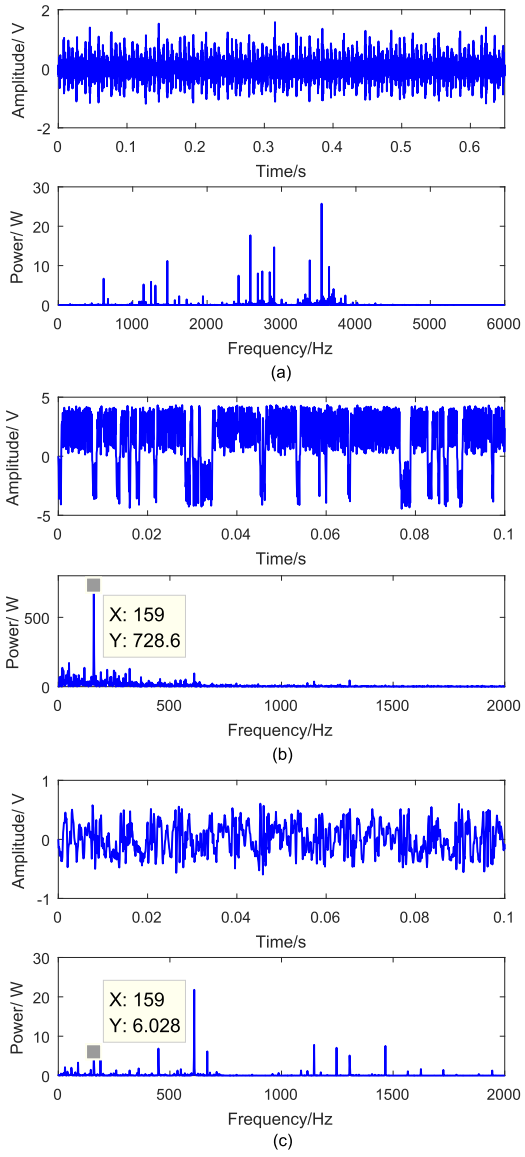

FIGURE 14. The inner race fault signal of the bearing drive end and the corresponding power spectra, (a) noisy signal; (b) the output signal of the NPWSR system; (c) the output signal of the CBSR system.

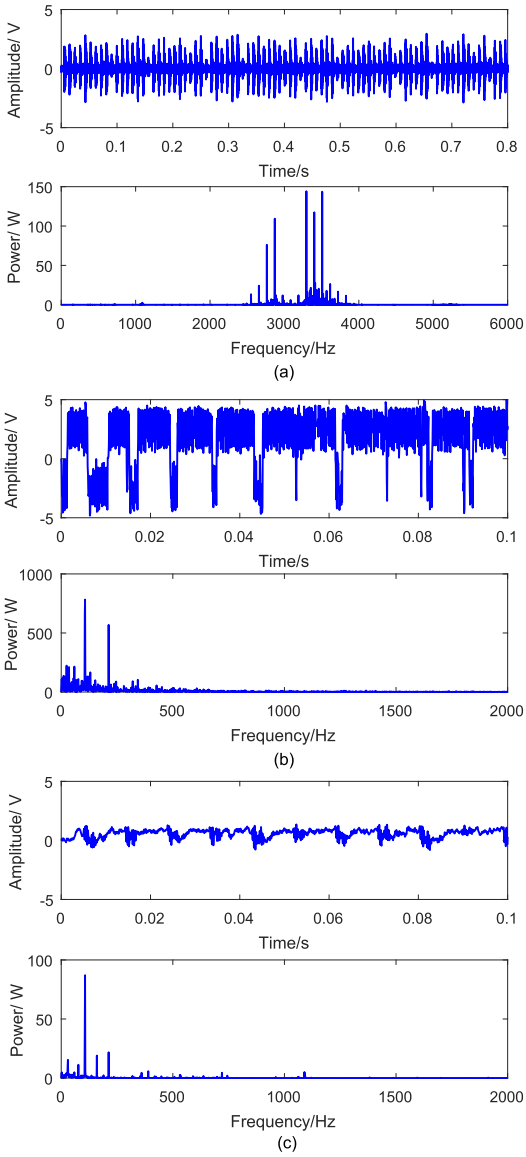

FIGURE 15. The outer race fault signal of the bearing drive end and the corresponding power spectra, (a) noisy signal; (b) the output signal of the NPWSR system; (c) the output signal of the CBSR system.

characteristic frequency of the novel potential well model is higher, and the interference component around the characteristic frequency is also smaller. The results indicate that the novel potential well model performs better than the classical bistable model in detecting the inner race fault signal, and the results verify the effectiveness of the NPWSR model in bearing fault diagnosis.

Fig. 15(a) plots the waveform of the bearing outer race fault signal and its power spectrum. In the time-domain diagram, the periodic characteristics cannot be clearly observed due to noise interference. In the power spectrum, the fault characteristic frequency component is not observed, and the frequency bands are mainly concentrated in 3000 Hz-4000 Hz. The sampling frequency is $f_s = 12$ kHz, the number of sampling points is $N = 10000$ and the input SNR is -55.65 dB. The bearing outer race fault signal is sent to the CBSR and NPWSR systems. The parameters of the two systems are $a = 2.4822$, $b = 0.105$, $l = 0.4197$ and $a_1 = 0.0955$, $b_1 = 0.1354$, respectively, according to the PSO optimization. The detection results are shown in Figs. 15(b) and 15(c). The output SNR of the novel potential well model is -21.13 dB, and the output SNR of the classical bistable model is -20.57sdB. Comparing the output time-domain diagrams of Figs. 15(b) and 15(c), the periodic characteristics of the novel potential well model are more obvious, and the output does not exhibit saturation. From the output power spectrum of Figs. 15(b) and 15(c), the spectral peak at the fault characteristic frequency of the novel potential well model is higher, and the second harmonic frequency can be clearly seen. The results indicate that the novel potential well model performs better in detecting the outer race fault signal, and the results verify the effectiveness of the proposed model in bearing fault diagnosis.

VI. CONCLUSION

The novel potential well model proposed in this paper is based on the advantages of a piecewise bistable potential SR model and an applied signal SR model. This model can effectively solve the problems of the output saturation and high barrier in the classical bistable model. The performance analysis results show that the SR system based on the novel potential well model achieves better detection performance than the classical bistable model. Finally, compared with the results of the classical bistable model, the experimental results show that the novel potential well model achieves a higher output SNR and a higher spectral peak at the characteristic frequency.

REFERENCES

[1] R. Benzi, A. Sutera, and A. Vulpiani, "The mechanism of stochastic resonance," *J. Phys. A, Math. Gen.*, vol. 14, no. 11, pp. L453–L457, 1981, doi: 10.1088/0305-4470/14/11/006.

[2] R. Benzi, G. Parisi, A. Sutera, and A. Vulpiani, "A theory of stochastic resonance in climatic change," *SIAM J. Appl. Math.*, vol. 43, no. 3, pp. 565–578, Jun. 1983, doi: 10.1137/0143037.

[3] L. Gammaitoni, P. Hänggi, F. Marchesoni, and P. Jung, "Stochastic resonance," *Rev. Mod. Phys.*, vol. 70, no. 1, pp. 223–287, Jan./Mar. 1998, doi: 10.1103/RevModPhys.70.223.

[4] S. Fauve and F. Heslot, "Stochastic resonance in a bistable system," *Phys. Lett. A*, vol. 97, no. 1, pp. 5–7, Aug. 1983, doi: 10.1016/0375-9601(83)90086-5.

[5] S. Mitaim and B. Kosko, "Adaptive stochastic resonance," *Proc. IEEE*, vol. 86, no. 11, pp. 2152–2183, Nov. 1998, doi: 10.1109/5.726785.

[6] B. H. Xu, F. Duan, R. Bao, and J. Li, "Stochastic resonance with tuning system parameters: The application of bistable systems in signal processing," *Chaos, Solitons Fractals*, vol. 13, no. 4, pp. 633–644, Mar. 2002, doi: 10.1016/s0960-0779(00)00266-6.

[7] D. Wu and S. Zhu, "Stochastic resonance in a bistable system with time-delayed feedback and non-Gaussian noise," *Phys. Lett. A*, vol. 363, no. 3, pp. 202–212, 2007, doi: 10.1016/j.physleta.2006.11.006.

[8] A. Das, N. G. Stocks, and E. L. Hines, "Enhanced coding for exponentially distributed signals using suprathreshold stochastic resonance," *Commun. Nonlinear Sci. Numer. Simul.*, vol. 14, no. 1, pp. 223–232, 2009, doi: 10.1016/j.cnsns.2007.07.013.

[9] J. W. Mo, S. Ouyang, and H. Xiao, "Study on application of array bistable stochastic resonance in weak signal detection," *Signal Process.*, vol. 27, no. 5, pp. 755–759, May 2011.

[10] H.-L. He, T.-Y. Wang, Y. Zhang, Q. Li, and Y.-G. Leng, "Study on nonlinear filter characteristic and engineering application of cascaded bistable stochastic resonance system," *Mech. Syst. Signal Process.*, vol. 21, no. 7, pp. 2740–2749, 2007, doi: 10.1016/j.ymssp.2007.02.004.

[11] H. Dong, H. Wang, X. Shen, and Z. Jiang, "Effects of second-order matched stochastic resonance for weak signal detection," *IEEE Access*, vol. 6, pp. 46505–46515, 2018, doi: 10.1109/ACCESS.2018.2866170.

[12] A. Kenfack and K. P. Singh, "Stochastic resonance in coupled underdamped bistable systems," *Phys. Rev. E, Stat. Phys. Plasmas Fluids Relat. Interdiscip. Top.*, vol. 82, no. 4, 2010, Art. no. 046224, doi: 10.1103/PhysRevE.82.046224.

[13] S. Lu, Q. He, F. Hu, and F. Kong, "Sequential multiscale noise tuning stochastic resonance for train bearing fault diagnosis in an embedded system," *IEEE Trans. Instrum. Meas.*, vol. 63, no. 1, pp. 106–116, Jan. 2014, doi: 10.1109/tim.2013.2275241.

[14] J. Li, J. Zhang, M. Li, and Y. Zhang, "A novel adaptive stochastic resonance method based on coupled bistable systems and its application in rolling bearing fault diagnosis," *Mech. Syst. Signal Process.*, vol. 114, pp. 128–145, Jan. 2019, doi: 10.1016/j.ymssp.2018.05.004.

[15] Y. Qin, Y. Tao, Y. He, and B. Tang, "Adaptive bistable stochastic resonance and its application in mechanical fault feature extraction," *J. Sound Vib.*, vol. 333, no. 26, pp. 7386–7400, Dec. 2014, doi: 10.1016/j.jsv.2014.08.039.

[16] L. Zhang, L. Cao, and D.-J. Wu, "Effect of correlated noises in an optical bistable system," *Phys. Rev. A.*, vol. 77, no. 1, 2008, Art. no. 015801, doi: 10.1103/PhysRevA.77.015801.

[17] H. Sasaki, S. Sakane, T. Ishida, T. Kitamura, R. Aoki, and M. Todorokihara, "Suprathreshold stochastic resonance in visual signal detection," *Behavioural Brain Res.*, vol. 193, no. 1, pp. 152–155, 2008, doi: 10.1016/j.bbr.2008.05.003.

[18] K. Sriram and M. S. Gopinathan, "Stochastic resonance in circadian rhythms," *Theor. Chem. Accounts*, vol. 114, nos. 1–3, pp. 46–51, 2005, doi: 10.1007/s00214-005-0642-3.

[19] Z. Deng, J. H. Cheong, C. Caranica, L. Wu, X. Qiu, M. T. Judge, B. Hull, C. Rodriguez, J. Griffith, A. Al-Omari, S. Arsenault, H.-B. Schüttler, L. Mao, and J. Arnold, "Single cells of neurospora crassa show circadian oscillations, light entrainment, temperature compensation, and phase synchronization," *IEEE Access*, vol. 7, pp. 49403–49417, 2019, doi: 10.1109/ACCESS.2019.2910731.

[20] Z. Qiao, Y. Lei, J. Lin, and F. Jia, "An adaptive unsaturated bistable stochastic resonance method and its application in mechanical fault diagnosis," *Mech. Syst. Signal Process.*, vol. 84, pp. 731–746, Feb. 2017, doi: 10.1016/j.ymssp.2016.08.030.

[21] H. B. Zhang, Q. He, S. Lu, and F. Kong, "Stochastic resonance with a joint woods-saxon and Gaussian potential for bearing fault diagnosis," *Math. Problems Eng.*, vol. 2014, Jun. 2014, Art. no. 315901, doi: 10.1155/2014/315901.

[22] G. Zhang and J. P. Gao, "Weak signal detection based on combination of power and exponential function model in tri-stable stochastic resonance," *J. Comput. Appl.*, vol. 38, no. 9, pp. 2747–2752, Jun. 2018, doi: 10.11772/j.issn.1001-9081.2018010192.

[23] Y. H. Xin and L. Z. Xue, "The study for the method to weak signal detection based on the combination of the chaotic ocillator system and stochastic resonance system," *Sci. J. Inf. Eng.*, vol. 4, no. 3, pp. 44–56, Jun. 2014.

[24] J. L. Duan, "Study on incipient fault diagnosis of machinery based on piecewise linearity and unsaturated stochastic resonance," *China Meas. Test*, vol. 43, no. 8, pp. 106–112, 2017, doi: 10.11857/j.issn.1674-5124.2017.08.022.

[25] L. He, X. Zhou, and T. Zhang, "Stochastic resonance characteristic analysis of new potential function under Levy noise and bearing fault detection," *Chin. J. Phys.*, vol. 56, no. 2, pp. 538–560, 2018, doi: 10.1016/j.cjph.2018.02.004.

[26] G. Zhang, D. Hu, and T. Zhang, "Stochastic resonance in unsaturated piecewise nonlinear bistable system under multiplicative and additive noise for bearing fault diagnosis," *IEEE Access*, vol. 7, pp. 58435–58448, 2019, doi: 10.1109/ACCESS.2019.2914138.

[27] Z.-H. Lai and Y.-G. Leng, "Generalized parameter-adjusted stochastic resonance of duffing oscillator and its application to weak-signal detection," *Sensors*, vol. 15, no. 9, pp. 21327–21349, 2015, doi: 10.3390/s150921327.

[28] Q. Ma, D. Huang, and J. Yang, "Adaptive stochastic resonance in second-order system with general scale transformation for weak feature extraction and its application in bearing fault diagnosis," *Fluctuation Noise Lett.*, vol. 17, no. 1, 2018, Art. no. 1850009.

[29] D. Han, P. Li, S. An, and P. Shi, "Multi-frequency weak signal detection based on wavelet transform and parameter compensation band-pass multi-stable stochastic resonance," *Mech. Syst. Signal Process.*, vols. 70–71, no. 3, pp. 995–1010, 2016, doi: 10.1016/j.ymssp.2015.09.003.

[30] B. Dybiec and E. Gudowska-Nowak, "Stochastic resonance: The role of alpha-stable noises," *Acta Phys. Polonica B*, vol. 37, no. 5, pp. 1479–1490, 2006.

[31] G. L. Zhang, X. L. Lü, and Y.-M. Kang, "Parameter-induced stochastic resonance in overdamped system with α stable noise," *Acta Phys. Sin.*, vol. 61, no. 4, 2014, Art. no. 040501, doi: 10.1016/j.ymssp.2015.09.003.

[32] Y. Wang, J. Shangbin, Z. Qing, L. Shuang, and Q. Xiaoxue, "A weak signal detection method based on adaptive parameter-induced tri-stable stochastic resonance," *Chin. J. Phys.*, vol. 56, no. 3, pp. 1187–1198, 2018, doi: 10.1016/j.cjph.2018.04.002.

[33] G. Zhang, Y. Zhang, T. Zhang, and J. Xiao, "Stochastic resonance in second-order underdamped system with exponential bistable potential for bearing fault diagnosis," *IEEE Access*, vol. 6, pp. 42431–42444, 2018, doi: 10.1109/ACCESS.2018.2856620.

[34] L. Tong, X. Li, J. Hu, and L. Ren, "A PSO optimization scale-transformation stochastic-resonance algorithm with stability mutation operator," *IEEE Access*, vol. 6, pp. 1167–1176, 2017, doi: 10.1109/ACCESS.2017.2778022.

[35] M. Lin, M. L. Zhang, and Y. M. Huang, "The stochastic energetics resonance of bistable systems and efficiency of doing work," *Acta Phys. Sin.*, vol. 60, no. 8, 2011, Art. no. 080509.

[36] J. Li, X. Chen, and Z. He, "Multi-stable stochastic resonance and its application research on mechanical fault diagnosis," *J. Sound Vibrat.*, vol. 332, no. 22, pp. 5999–6015, Oct. 2013, doi: 10.1016/j.jsv.2013.06.017.
[37] Z. Gingl, P. Makra, and R. Vajtai, "High signal-to-noise ratio gain by stochastic resonance in a double well," *Fluctuation Noise Lett.*, vol. 1, no. 3, pp. L181–L188, 2001, doi: 10.1142/S0219477501000408.

SHANGBIN JIAO was born in 1974. He received the B.S., M.S., and Ph.D. degrees from the College of Automation and Information Engineering, Xi'an University of Technology, Xi'an, in 1997, 2002, and 2006, respectively. He is currently a Professor and the Ph.D. Supervisor with the Xi'an University of Technology. His general research interests include weak signal detection, device intelligence status detection, and early fault diagnosis.

SHUANG LEI was born in 1995. She received the B.S. degree from the College of Automation and Information Engineering, Xi'an University of Technology, Xi'an, in 2017, where she is currently pursuing the M.S. degree in automation and information engineering. Her main research interests include stochastic resonance and weak signal detection.

WEI JIANG was born in 1996. She received the B.S. degree from the College of Automation, Xi'an University of Posts and Telecommunications, Xi'an, in 2017, where she is currently pursuing the M.S. degree in automation and information engineering. Her main research interests include chaos and weak signal detection.

QING ZHANG was born in 1974. She received the B.S. and M.S. degrees from the College of Automation and Information Engineering, Xi'an University of Technology, Xi'an, in 1997 and 2007, respectively. She is currently a Senior Engineer with the Engineering Research Center, Xi'an University of Technology. Her main research interests include fault diagnosis and weak signal detection.

WEICHAO HUANG was born in 1984. He received the B.S. degree from the Xi'an University of Engineering, in 2007. He received the M.S. and Ph.D. degrees from the Xi'an University of Technology, in 2012 and 2018, respectively. He is currently with the School of Automation and Information Engineering, Xi'an University of Technology. His general research directions are weak signal detection, complex system modeling, and intelligent optimization.